THE JOURNAL OF PHYSICAL CHEMISTRY A

Article

Cite This: J. Phys. Chem. A 2019, 123, 5378−5387

pubs.acs.org/JPCA

Bond-Dependent Thole Model for Polarizability and Spectroscopy

Mark DelloStritto,[†,‡] Michael L. Klein,[†,¶,‡] and Eric Borguet*[,†,‡]

[†]Department of Chemistry, [‡]Center for the Complex Materials, and [¶]Institute for Computational Molecular Science, Temple University, Philadelphia, Pennsylvania 19122, United States

Supporting Information

ABSTRACT: We present a new model for the calculation of molecular polarizabilities from effective atomic polarizabilities. This model is based on the Thole modified dipole interaction model for molecular polarizabilities, where the total polarizability is computed as a sum of effective atomic polarizabilities modified by dipole−dipole interactions. We extend this model by making the atomic polarizabilities explicit functions of the interatomic distances, scaling them by the radius of the volume an atom occupies in a molecule. We use the SCAN functional to show that this model, denoted TholeL, yields accurate molecular polarizabilities with little dependence on the training set. We also demonstrate that the TholeL model yields accurate polarizabilities for configurations far from the ground state structure for a wide range of molecules. Finally, we show that the TholeL model can be used to generate accurate Raman spectra for water, crystalline urea, and urea in water from ab initio molecular dynamics simulations.

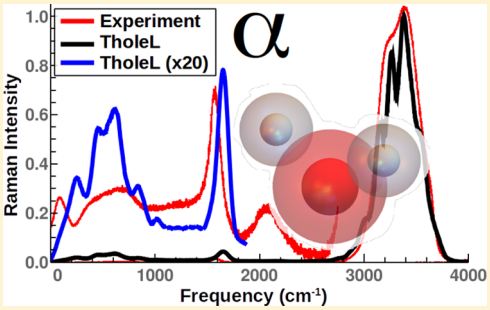

INTRODUCTION

The calculation of atomic and molecular polarizabilities is an essential component of a wide range of theoretical models and is necessary for the calculation of an equally large number of experimental observables. In the field of molecular dynamics, it has long been recognized that static charges do not adequately model the fluctuating electric field in and around molecules, and so various polarizable force fields have been introduced. These force fields can range from simple additive models[1] to Drude oscillators[2] to Gaussian-smeared atomic charges.[3] These models have generally been shown to improve both the electrostatic properties and equilibrium structures over non-polarizable force fields.[4] The polarizability is also key in devising QM/MM strategies for extending the range of applicability of ab initio methods.[5] Finally, the polarizability is important for predicting vibrational spectra, including both Raman scattering[6] and sum frequency generation.[7,8]

While there are well-established ab initio methods for calculating the polarizability at high accuracy, in most cases, these approaches are prohibitively expensive. Although it is relatively simple to compute the polarizability from analytic derivatives of the Hamiltonian, accurate values of the polarizability often require very large basis sets.[9] It is not uncommon to require triple or quadruple zeta basis sets to obtain accurate results, and even then polarization and diffuse functions are often necessary for the polarizability to converge.[10] Not only do these basis sets require more computation time, but the addition of diffuse functions can complicate convergence, necessitating more robust and more expensive optimization algorithms. Finally, in many cases, density functional theory (DFT) is the common choice for moderately sized molecules, but problems with describing electron correlation make DFT impractical for polarizability calculations.[11] Thus, one must at least use DFT with some exact exchange added, further adding to the cost of the calculation.

Owing to the prohibitive cost of polarizability calculations, there is a long history of approximate models of the molecular polarizability. Although much use has been made of bond models, atomic models of the polarizability tend to be more flexible and thereby more common. The earliest atomic models involved simply summing over parameterized atomic polarizabilities, and despite the simplicity of such an approach, these models tend to reproduce the average polarizability quite well.[12] Such models are not very flexible, however, with parameters depending on both the local bonding environment and the size and composition of the training set.[13] In order to ensure the accuracy and general applicability, large training sets with very accurate molecular geometries are required.

The accuracy and generality of polarizability models was improved significantly with the introduction of dipole interactions. The atom dipole interaction (ADI) model for the polarizability was first introduced by Silberstein[14] and was later refined by Applequist, Carl, and Fung.[15] These authors recognized that they could obtain polarizabilities that are self-consistent with intramolecular electric fields by including the dipole interaction tensor into their polarizability calculations. While this approach was mildly successful, it required very small atomic polarizability parameters due to the divergence of the dipole−dipole interaction at small distances. This model was significantly improved by Thole,[16] who removed this divergence by replacing the point dipoles at each atom with

Received: December 13, 2018
Revised: April 23, 2019
Published: June 13, 2019

DOI: 10.1021/acs.jpca.8b12011
J. Phys. Chem. A 2019, 123, 5378−5387

smeared out charge densities. The Thole model has seen widespread use in molecular simulation,[3] has been shown to maintain accuracy for large data sets,[17] has been expanded to hyperpolarizability calculations,[18] and has been extended to include both dipole interactions from both Slater-like and Gaussian-like charge densities.[19,20]

Despite the success of the ADI model, such models are generally limited to studying molecules at their ground-state geometries. The dependence of molecular polarizability on the atomic position in ADI models arises from the change in the total charge density contributing to the dipole−dipole interaction with changes in bond length and angle. As the bond length increases, more of the model charge density around a given atom is included in the dipole−dipole interaction tensor, and so the dipole interaction and the effective polarizabilities increase. While this leads to qualitatively correct dependence of the polarizability on molecular geometry, the gradient of the polarizability with respect to atomic positions is often underestimated. This can often result in problems, including dependence on the details of the training set and difficulty predicting the relative weights of vibrational spectra. While ADI models can be used for vibrational spectroscopy,[21] they are generally restricted to narrow frequency ranges and relatively homogeneous systems where all vibrational chromophores have similar frequencies and polarizabilities.

In this work, we improve upon the ADI model by introducing atomic radius-dependent polarizabilities, which reproduce the dependence of the molecular polarizability on atomic configurations. One of the reasons that a simple, additive model for the polarizability can work so well is that, in atomic units, the polarizability has units of a_0^3. The polarizability of a molecule should then be proportional to the size of the molecule, and thus in turn it should be proportional to the number of atoms in the molecule. We can take advantage of this same scaling of the polarizability to improve upon ADI models by making the atomic polarizabilities depend on the radius of the spherical "volume" occupied by the atom in the molecule. While the dependence of the polarizability on molecular geometry is a complex function of the changing hybridization of the molecular orbitals, it is useful to think of the atomic charge densities simply being stretched or compressed to occupy large or smaller spherical volumes, respectively, in the deformed molecule. The atomic polarizability will then scale correspondingly with the volume, growing and shrinking with changes in the atomic volume. In practice, however, we find that the polarizability should scale with the radius of the atomic volume in order to best reproduce the molecular polarizability. Despite the simplicity of such an approach, we show that this picture allows us to accurately predict the polarizability of a wide range of molecules up to the dissociation limit.

We train this model, denoted TholeL for bond length-dependent Thole model, on the TABS database[22] and find that it can accurately reproduce the ab initio polarizability. We show that this model yields accurate polarizabilities not only for molecules at the ground state but also for molecular geometries far from equilibrium. Finally, with an accurate model of the polarizability as a function of the molecular geometry over such a wide range, we show that it is possible to efficiently calculate Raman spectra from ab initio trajectories for a wide range of systems.

THEORY

While the details of ADI models are described elsewhere, we summarize the general approach in order to introduce the expansion to volume-dependent polarizabilities. The starting point for all ADI models is the equation for the self-consistent dipole in a system of atoms interacting under the dipole approximation

$$\mu_i = \alpha_i(E_i + T_{ij}\,\mu_j) \tag{1}$$

where μ_i and α_i are the dipole moments and polarizabilities of the ith atom, E_i is the external field at the ith atom, and T_{ij} is the dipole interaction tensor, which gives the electric field at the ith atom due to the jth atom. Note that we use Einstein notation, such that all repeated indices are implicitly summed. By inverting the above equation, one obtains

$$\alpha_i^{-1}\mu_i - T_{ij}\,\mu_j = E_i \tag{2}$$

Equation 2 can be written as a matrix equation $A\mu = E$, where the matrix A has the form of an inverse polarizability. We can thus define an effective polarizability α_i^{eff} as

$$\alpha_i^{\text{eff}} = \sum_j (A^{-1})_{ij} \tag{3}$$

In Thole's initial approach, the dipole interaction tensor was calculated from a single H atom-like charge density.[16] Since the charge density, and thereby the dipole interaction tensor, is determined by a single exponential function, we denote this as the "expontential" or "Exp" interaction. The dipole interaction tensor is then

$$T_{ij} = 3r_{ij}r_{ij}^{\mathrm{T}}/r_{ij}^{5}\left[1 - \left(\frac{1}{6}b_{ij}^{3} + \frac{1}{2}b_{ij}^{2} + b_{ij} + 1\right)e^{-b_{ij}^{2}}\right] - Ir_{ij}^{\mathrm{T}}r_{ij}/r_{ij}^{3}\left[1 - \left(\frac{1}{2}b_{ij}^{2} + b_{ij} + 1\right)e^{-b_{ij}^{2}}\right] \tag{4}$$

where $r_{ij} \equiv r_i - r_j$, r_{ij}^{T} is the transpose of r_{ij}, and I is the identity matrix. Here, $b_{ij} \equiv ar_{ij}(\alpha_i\alpha_j)^{1/6}$ is a scaling factor, and a is a free parameter determined by fitting to ab initio data.

In this work, we also use a dipole interaction tensor based on the interaction between two Gaussian charge densities:[23]

$$T_{ij} = \frac{(3r_{ij}r_{ij}^{\mathrm{T}} - Ir_{ij}^{\mathrm{T}}r_{ij})}{|r_{ij}|^5}\left[\mathrm{erf}(|r_{ij}|/R_{ij}) - \frac{2}{\pi}e^{-(|r_{ij}|/R_{ij})^2}\right] - \frac{4}{\sqrt{\pi}R_{ij}^{3}}e^{-(|r_{ij}|/R_{ij})^2}\frac{r_{ij}r_{ij}^{\mathrm{T}}}{|r_{ij}|^2} \tag{5}$$

In this case, the scaling factor R_{ij} is defined by effective atomic radii $R_{ij} \equiv \sqrt{R_i^2 + R_i^2}$, where R_i is a radius defined by

$$R_i \equiv \left(\frac{2}{3\sqrt{\pi}}\alpha_i\right)^{1/3} \tag{6}$$

The atomic radius is defined in terms of the atomic polarizability by taking the limit $r_{ij}\to 0$, leaving a constant term[24] $4/(3\sqrt{\pi})R_{ij}^{-3}$. We interpret this constant term as twice the self-energy of a single dipole, since the interaction as $r_{ij}\to 0$ gives the interaction between two dipoles at zero distance. Since the interacting Gaussian charges give rise to a term with an error function, we denote eq 5 as the "Erf" dipole interaction.

DOI: 10.1021/acs.jpca.8b12011
J. Phys. Chem. A 2019, 123, 5378−5387

In most approaches, the initial polarizabilities α_i are parameters determined from a fitting procedure to a large set of ab initio molecular polarizabilities. The polarizabilities α_i are then static properties of the atoms, and all changes in the molecular polarizability with respect to the atomic coordinates are due to changes in the dipole interaction tensor T_{ij}. However, the changes in T_{ij} are not large enough to accurately represent the changes in the molecular polarizability with respect to changes in the molecular geometry.

In order to rectify this deficiency in the ADI model, we make the polarizability α_i an explicit function of the size of the atom in a molecule. This strategy is inspired by the atom-in-molecules approach to molecular properties and by the fact that the polarizability has units of a_0^3. The reasoning is that, as a bond is stretched or compressed, the atom-in-molecule is able to occupy a larger or smaller volume, respectively, assuming that the overlapping charge densities repel each other due to electrostatic effects and Fermi degeneracy. While this is obviously not a correct picture of the electronic structure of a molecule, it employs similar ideas of atomic volume employed in Hirshfeld[25] and Bader partitioning[26] to find atomic charges and polarizabilities.

We define the change in the atomic radius, and thereby the atomic volume, in a given molecule via the overlap of atomic radii. We take the vacuum atomic radius to be the covalent atomic radius. When the two atoms i and j are near each other, we calculate a new radius for atom i as

$$R_i \equiv R_i^{(0)} - 0.5(R_i^{(0)} + R_j^{(0)} - r_{ij}) \tag{7}$$

where $R_i^{(0)}$ is the covalent radius of atom i, R_i is the new radius, and r_{ij} is the distance between the two atoms. If we define the radius R_j for atom j in the same way, then R_i and R_j, by definition, point toward the other atomic center along a line connecting the two, such that the vectors meet at the plane of intersection of two spheres with radii $R_i^{(0)}$ and $R_j^{(0)}$. This process is illustrated in Figure 1, where we can see that the vectors R_i and R_j result in atomic radii which touch at only a single point between atoms i and j.

We perform the above procedure for every atom in a system, where for atom i, we define a new radius vector R_i using the nearest neighbor, even if it is greater than the covalent radius $R_i^{(0)}$. In this way, we ensure that the volume of each atom in a molecule has a minimal overlap with its nearest neighbor. In other words, the sphere formed by R_i must touch the sphere formed by the nearest-neighbor radius R_j at a single point. This effectively means that the volume of an atom in a molecule is determined by its nearest neighbor in the molecule, whether it is expanded or contracted with respect to its vacuum value. Such a procedure is obviously incorrect for a dissociating bond in vacuum, but for systems where no bonds are broken this procedure gives a good measure of the volume occupied by an atom-in-molecule and yields excellent results for the molecular polarizability, as shown below.

Finally, once we have a new radius vector R_i, we can scale the polarizability α_i. Since the polarizability has units of a_0^3, one might assume that it is best to scale α_i by the cube of the ratio of R_i with the covalent radius $R_i^{(0)}$. However, we find that this results in an overestimation of the dependence of the polarizability on the bond length; rather, it is best to scale the polarizability with respect to the ratio $R_i/R_i^{(0)}$. While it is not immediately clear why this is the case, note that we are scaling atom-in-molecule polarizabilities, which we then use to compute the molecular polarizability using the Thole model. The emperically observed linear relationship between polarizability and volume has primarily been observed with molecules, such that all complex interatomic interactions are implicitly included.[27] Thus, in order to better reflect the geometry of the molecule, we scale each diagonal component of the vacuum polarizability α_i by the ratio of the components of the ratio $R_i/R_i^{(0)}$. The scaled polarizability can thus be written as

$$(\alpha_i')_{nn} = (\alpha_i)_{nn} \cdot (R_i/R_i^{(0)})_n \tag{8}$$

Note that by scaling the polarizability by the components of the ratio $R_i/R_i^{(0)}$, we are essentially accounting for the stretching or compressing of a bond between two atoms. Once the scaled polarizabilities are obtained, we follow the standard procedure of ADI methods to find the effective polarizabilities, namely, using eqs 2 and 3 but with α_i' replacing α_i.

When we scale the polarizabilities, a subtle issue arises because the atomic radius in eq 6 is defined by taking the interatomic distance to zero, resulting in a finite interaction energy at zero distance when using static polarizabilities. However, if we scale the polarizabilities using the interatomic distance as in eq 8, the polarizabilities and the scaling constant should go to zero as the interatomic distance goes to zero. While this results in a divergent dipole−dipole interaction, since T_{ij} and α_i^{-1} both scale as R_{ij}^{-1} as the distance $r_{ij}\to 0$, the resulting effective polarizabilities go to zero as $r_{ij}\to 0$. Without a finite dipole−dipole interaction as $r_{ij}\to 0$, one cannot use eq 6 to compute the scaling constant.

Despite this issue, we elect to continue to use eq 6 to define the atomic radius for the "Erf" interaction using the scaled polarizabilities. Our reasoning is that our scaling of the

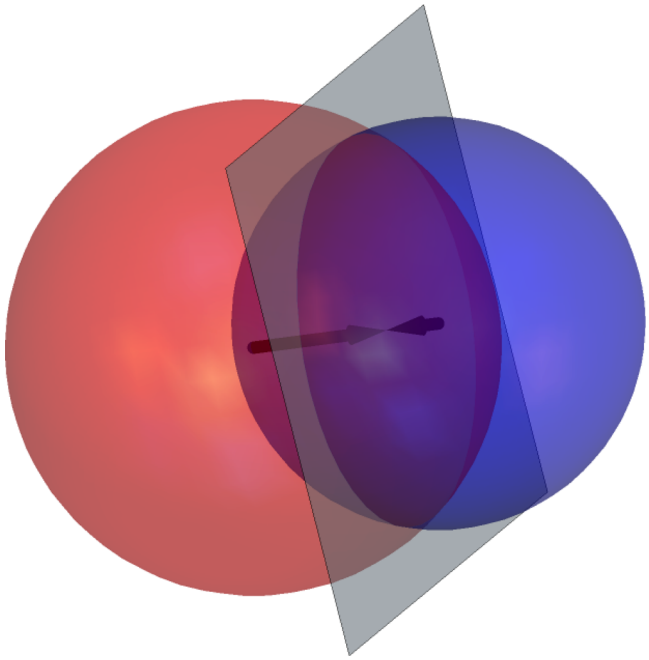

Figure 1. Illustration of the new radii determined by eq 7 for a diatomic molecule. The spheres represent the original, covalent radii, while the spheres formed by the new radii, which have minimal overlap, are not shown. The gray plane shows the intersection between the two spheres, and the two arrows show the point at which they meet.

DOI: 10.1021/acs.jpca.8b12011
J. Phys. Chem. A 2019, 123, 5378−5387

polarizabilities is simply a method to generate the polarizability parameters that work for every reasonable configuration of a molecule, which we might expect to see in, for example, a molecular dynamics simulation, rather than just the equilibrium configuration. Once these scaled parameters are found for a given molecular configuration, we then freeze the polarizabilities and the fictitious charge densities used to compute the dipole−dipole interactions and let the interatomic distance $r_{ij}\rightarrow 0$. We thus recover eq 6 for a large number of configurations of a molecule but with the scaled polarizabilities. Indeed, in order to obtain eq 6, even without scaling the polarizabilities, one must assume that the charge density generating the dipole−dipole interaction is unchanged as $r_{ij}\rightarrow 0$. Note that this approach is also supported by numerical evidence: we attempted to define the scaling parameter as $R_{ij} = a(\alpha_i^{2/3} + \alpha_j^{2/3})^{1/2}$, where a is a global scaling constant similar to that used in eq 4. Fitting the global parameter a to ab initio data yielded a factor close to that yielded by eq 6. Thus, we believe that our use of eq 6 with the scaled polarizabilities is justified.

The parallel and perpendicularly reduced scattered Raman spectra are calculated using the following time-dependent formalism[6]

$$\begin{aligned} I_{\parallel}(\omega) &= \frac{\omega}{(\omega-\omega_I)^4}\left(1-\exp\left(-\frac{\hbar\omega}{k_B T}\right)\right)Q(\omega) \\ &\quad \int_{-\infty}^{\infty} dt e^{-i\omega t}\frac{1}{15}\langle 15\bar{\alpha}(t)\bar{\alpha}(0) + 2\mathrm{Tr}[\beta(t)\beta(0)]\rangle \\ I_{\perp}(\omega) &= \frac{\omega}{(\omega-\omega_I)^4}\left(1-\exp\left(-\frac{\hbar\omega}{k_B T}\right)\right)Q(\omega) \\ &\quad \int_{-\infty}^{\infty} dt e^{-i\omega t}\frac{1}{10}\langle \mathrm{Tr}[\beta(t)\beta(0)]\rangle \end{aligned} \tag{9}$$

where $\bar{\alpha}(t) \equiv (1/3)\mathrm{Tr}[\alpha(t)]$, Tr is the trace, $\beta \equiv \bar{\alpha} - \alpha I$ is the anisotropic part of the polarizability operator, ω_I is the incident radiation frequency, $Q(\omega)$ is a quantum correction factor, and k_B is Boltzmann's constant. Note that the factor of $(\omega-\omega_I)^{-4}$ comes from the definition the reduced Raman spectrum, which ensures that the computed Raman spectrum is directly proportional to the intrinsic Raman scattering activity.[28] The quantum correction factor guarantees that the above expressions satisfy the detailed balance condition $I(\omega) = \exp(\hbar\omega/k_B T)I(-\omega)$. We use the harmonic approximation $Q_{HA}(\omega) = \hbar\omega/k_B T/(1-\exp(-\hbar\omega/k_B T))$ as this yields the best results in most cases and obeys the fluctuation dissipation theorem.[29] The expressions for the intensity in this case then become

$$\begin{aligned} I_{\parallel}(\omega) &= (\omega-\omega_I)^{-4}\omega^2\int_{-\infty}^{\infty} dt e^{-i\omega t}\frac{1}{15}\langle 15\bar{\alpha}(t)\bar{\alpha}(0) \\ &\quad + 2\mathrm{Tr}[\beta(t)\beta(0)]\rangle \\ I_{\perp}(\omega) &= (\omega-\omega_I)^{-4}\omega^2\int_{-\infty}^{\infty} dt e^{-i\omega t}\frac{1}{10}\langle \mathrm{Tr}[\beta(t)\beta(0)]\rangle \end{aligned} \tag{10}$$

where we have removed the constant prefactors for brevity. In order to simplify our calculations, particularly to reduce noise at low frequencies, we use the properties of the time derivative of the Fourier transform to write the intensities in terms of the time derivative of the polarizability:

$$\begin{aligned} I_{\parallel}(\omega) &\sim (\omega-\omega_I)^{-4}\int_{-\infty}^{\infty} dt e^{-i\omega t}\frac{1}{15}\langle 15\dot{\bar{\alpha}}(t)\dot{\bar{\alpha}}(0) \\ &\quad + 2\mathrm{Tr}[\dot{\beta}(t)\dot{\beta}(0)]\rangle \\ I_{\perp}(\omega) &\sim (\omega-\omega_I)^{-4}\int_{-\infty}^{\infty} dt e^{-i\omega t}\frac{1}{10}\langle \mathrm{Tr}[\dot{\beta}(t)\dot{\beta}(0)]\rangle \end{aligned} \tag{11}$$

Since the polarizabilities in any physically realistic system with a constant number of particles oscillate around an average value, eq 11 guarantees a signal with zero mean, thereby guaranteeing the Fourier transform decays to zero at zero frequency. This approach avoids issues with numerical accuracy where small frequencies $\omega \approx 0$ are multiplied by the time average of the correlation functions in eq 10.

COMPUTATIONAL DETAILS

All polarizability calculations were performed using the Gaussian16 (rev. A.03)[30] software package. We used the ωB97XD functional[31] with the aug-cc-pVTZ basis set,[32,33] as this combination has been shown to yield accurate polarizabilities for the TABS database.[11] The optimized geometries were taken from the TABS database and were not modified for the polarizability calculations. We optimized the polarizability parameters for the TholeL model using the NLopt library[34] with the "Subplex" algorithm,[35] as it is a highly robust optimization algorithm.

In order to test the TholeL model for nonequilibrium geometries, we generated quasi-random configurations of a small subset of the TABS database. These geometries were generated by running Car−Parinello molecular dynamics (CPMD) simulations of the molecules using the B3LYP[36,37] functional in combination with the cc-pVDZ basis set, as we do not require high accuracy for the resulting geometries. After running each simulation for 0.5 ps with a step size of 0.5 fs, we sampled the trajectories every 25 fs and calculated the polarizability for each frame.

In order to test the TholeL model for Raman spectra calculations, we ran several simulations of crystalline systems. All trajectories were obtained using the "cp.x" module of Quantum Espresso (v.6.2.1).[38,39] For all simulations, we used CPMD with the HSCV pseudopotentials,[40,41] an electron mass of 100 a.u., a timestep of 2.0 a.u. while sampling the trajectories every ten steps (~0.5 fs), and a temperature of 300 K. We used the SCAN functional[42] for all simulations. Every simulation was equilibrated using velocity rescaling followed by equilibration with a Nose−Hoover thermostat.[43,44]

We ran the following simulations in order to test the TholeL model for Raman spectroscopy calculations of molecules. We ran an NVE simulation of liquid water using 32 H_2O molecules with a plane-wave cutoff of 90.0 Ry for 30 ps. We ran an NVE simulation of a single urea molecule solvated by 32 H_2O molecules with a plane-wave cutoff of 90.0 Ry for 30 ps. We ran an NVE simulation of crystalline urea using 16 urea molecules with a plane-wave cutoff of 130.0 Ry for 20 ps. Further simulation details are included in the Supporting Information.

DOI: 10.1021/acs.jpca.8b12011
J. Phys. Chem. A 2019, 123, 5378−5387

RESULTS AND DISCUSSION

We parameterized the TholeL model and the Thole model, without bond-dependent polarizabilities, on the TABS database using both the "Exp" dipole tensor (eq 4) and the "Erf" dipole tensor (eq 5). We chose to parameterize and test our model on the TABS database[22] as it is a reasonably large database, containing 1641 molecules, which features a wide range of common organic molecules up to a reasonably large size (34 atoms). Thorough testing of a small subset of the database has shown that accurate polarizabilities can be obtained using the ωB97XD functional coupled with the aug-cc-pVTZ basis set.[11] We parameterize both models, Thole and TholeL, by reducing the average of the norm of the difference between the ab initio and approximate polarizabilities

$$\chi = \frac{1}{N}\sum_i \sqrt{|\alpha_i^{(0)} - \alpha_i|^2} \tag{12}$$

where N is the total number of molecules, $\alpha_i^{(0)}$ is the ab initio polarizability of the ith molecule, and α_i is the approximate polarizability of the ith molecule. We use a random third of the TABS database to train our model, and the remaining two-thirds to test the resulting model.

We list the statistics of the error for the optimization of the $\alpha_i^{(0)}$ using the TABS database in Table 1 and show the correlation between the norms of the exact and approximate polarizabilities in Figure 2. In Table 1, we list the average error and the slope (M) and the correlation coefficient (R^2) for the exact and approximate polarizabilities. As we compute the full polarizability tensor for each molecule, we calculate the quantities mentioned above for the norm of the polarizability, the average polarizability, and the anisotropy of the polarizability. The norm is computed as $|\alpha| = \sqrt{\sum_{ij} \alpha_{ij}^2}$, the average is computed as $\langle\alpha\rangle = 1/3\sum_i \alpha_{ii}$, and the anisotropy is computed as $\delta = 9/2(\langle\alpha^2\rangle - \langle\alpha\rangle^2)$.[45]

All models yield accurate results for each of the measures chosen. The "Erf" interaction yields significantly more accurate off-diagonal elements as compared to "Exp", as evidenced by the lower error for the anisotropy, but also yields slightly worse average polarizabilities. Note that, while the Thole and TholeL methods yield very similar results, the TholeL model is slightly less accurate. This is mostly due to large molecules that are approximately 1D or 2D, such as anthracene, as the TholeL model tends to underestimate the longitudinal polarizability of the molecule. This is because the TholeL model tends to reduce the effective polarizabilities of atoms in molecules near the ground-state configuration, whereas the effective polarizabilities of the Thole model tend to remain close to their initial values. For molecules like anthracene, the Thole molecular polarizability is very close to a simple sum over atomic polarizabilities, and so the longitudinal polarizability is quite large and grows approximately linearly with the size of the molecule. For the TholeL model, on the other hand, if any atoms have relatively short bonds compared to the rest of the dataset, their effective polarizability can be significantly reduced compared to the initial value, thereby resulting in an underestimation of the longitudinal polarizability. We show this explicitly for five molecules in the TABS database with the largest polarizabilities in Tables 2 and 3, which show the average polarizability and anisotropy of the polarizability, respectively, for each molecule and for each model. Note that the TholeL model slightly underestimates the average

Table 1. Statistics of the Error of the Fit to the TABS Database, Including the Average Error and the Slope (M) and R^2 Coefficient of the Correlation between the Exact and Approximate Values[a]

parameters	Exp	Exp-L	Erf	Erf-L
err-$\|\alpha\|$	8.60	10.2	9.82	11.6
err-$\langle\alpha\rangle$	2.76	3.79	3.62	4.59
err-δ	5.40	6.15	5.44	6.26
M-$\|\alpha\|$	0.93	0.92	0.91	0.90
M-$\langle\alpha\rangle$	0.94	0.93	0.92	0.91
M-δ	0.85	0.84	0.92	0.89
R^2-$\|\alpha\|$	0.97	0.96	0.97	0.94
R^2-$\langle\alpha\rangle$	0.98	0.96	0.96	0.94
R^2-δ	0.91	0.88	0.93	0.89

[a] $|\alpha|$, $\langle\alpha\rangle$, and δ refer to the absolute differences (a.u.) for the norm, average polarizability, and anisotropy for the molecules in the TABS database, respectively. The "Exp" and "Erf" dipole interactions are defined in the text.

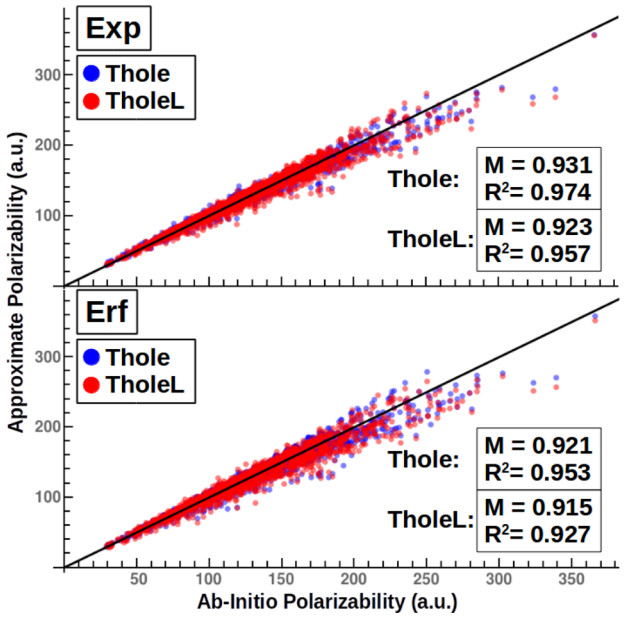

Figure 2. Correlation plots of the norms of the ab initio and approximate polarizabilities of the TABS database for the Thole and TholeL models for both the "Exp" and "Erf" interactions. The blue points show the results from the Thole model, while the red points show the results from the TholeL model.

Table 2. Average α (a.u.) of Five Molecules in the TABS Database with the Largest Polarizabilities[a]

name	exact	Thole-Exp	TholeL-Exp	Thole-Erf	TholeL-Erf
cinnamaldehyde	122	92	86	100	95
(*E*)-1,3,5-hexatriene	94	64	61	73	69
azulene	130	94	89	102	98
heptalene	153	113	103	125	121
phenazine	169	123	117	136	132
anthracene	179	129	121	141	135

[a] The "Exp" and "Erf" dipole interactions are defined in the text.

DOI: 10.1021/acs.jpca.8b12011
J. Phys. Chem. A 2019, 123, 5378−5387

Table 3. Anisotropy of α (a.u.) of Five Molecules in the TABS Database with the Largest Polarizabilities[a]

name	exact	Thole-Exp	TholeL-Exp	Thole-Erf	TholeL-Erf
cinnamaldehyde	115	21	12	93	81
(*E*)-1,3,5-hexatriene	102	13	8	75	62
azulene	109	21	13	91	84
heptalene	112	22	19	88	84
phenazine	169	32	21	138	127
anthracene	172	34	24	138	125

[a]The "Exp" and "Erf" dipole interactions are defined in the text.

polarizability and the anisotropy of the polarizability compared to the Thole model.

We further test the generality of the Thole and TholeL models by comparing their performance for nonequilibrium geometries of molecules. For a small subset of molecules in the TABS database (see the Supporting Information), we run CPMD simulations of each molecule to generate a series of random perturbations to the ground-state geometry, with an average standard deviation of the polarizability of ~3 bohr^3 for each molecular configuration. We then calculate approximate polarizabilities of these geometries using parameters obtained from training to the entire TABS database. The correlation plots (Figure 3) show that the TholeL model improves on the Thole model. Note that, in particular, although the Thole polarizabilities roughly follow a line of unit slope overall, the plot is composed of a series of overlapping horizontal lines. This indicates that, while the Thole model yields accurate average polarizabilities for each molecule, it does not, in general, yield quantitatively accurate derivatives of the polarizability with respect to atomic positions. On the other hand, the TholeL data is composed of a series of overlapping diagonal lines, indicating that the TholeL model yields accurate average polarizabilities and polarizability derivatives for each molecule. We can make this analysis more formal by looking at the mean slope and R^2 for each correlation plot for each molecule, as listed in Table 4. While there are still inaccuracies in the TholeL model, Table 4 shows that it greatly improves the polarizability derivatives over the Thole model.

Table 4. Average M and R^2 for the Polarizabilities of Each Set of Configurations for Each Molecule in the Subset of the TABS Database Used To Generate Random Configurations[a]

model	$\langle M \rangle$	$\langle R^2 \rangle$
Thole-Exp	0.117	0.362
TholeL-Exp	0.417	0.569
Thole-Erf	0.286	0.712
TholeL-Erf	0.586	0.745

[a]The "Erf" and "Exp" dipole interactions are defined in the text.

In order to compare the performance of the two models with respect to molecular configuration in more detail, we consider two specific examples. The first example is H_2O, as it is such an important molecule, and accurate models of its polarizability can significantly improve statistical quantities in MD simulations.[3] We plot the polarizability of H_2O predicted by the Thole and TholeL models with respect to the ab initio polarizability in Figure 4, where each r(OH) distance is set to 0.9575 Å and is varied within [−0.3 Å,0.2 Å] with a step of 0.025 Å and the θ(HOH) angle is set to 104.5° and is varied within [− 40°,40°] with a step of 5°. Figure 4 shows that the Thole model can, at times, yield quantitatively accurate polarizability derivatives near the equilibrium configuration. However, in most cases, the Thole model yields neither quantitatively accurate polarizabilities nor derivatives of the polarizability with respect to internal atomic coordinates, as is

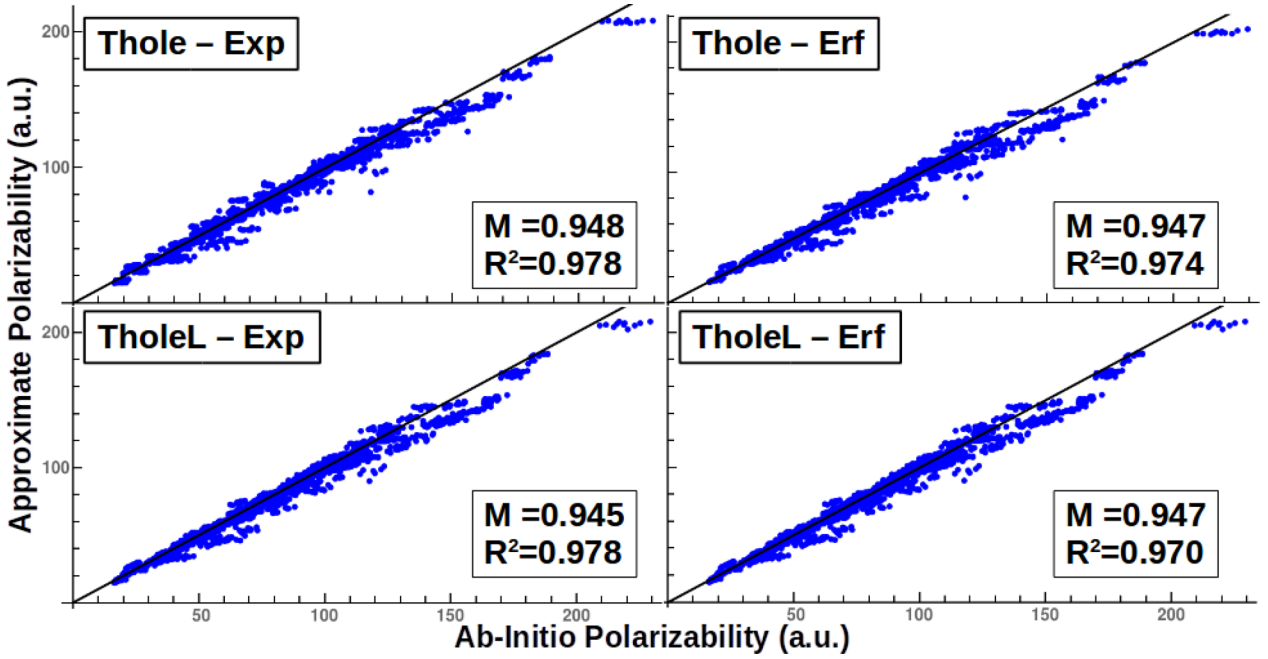

Figure 3. Correlation plots of the norms of the ab initio and approximate polarizabilities of random perturbations of a subset of molecules in the TABS database. Each panel shows the results using either the Thole or TholeL model with either the "Exp" or "Erf" dipole interaction, as defined in the text.

DOI: 10.1021/acs.jpca.8b12011
J. Phys. Chem. A 2019, 123, 5378−5387

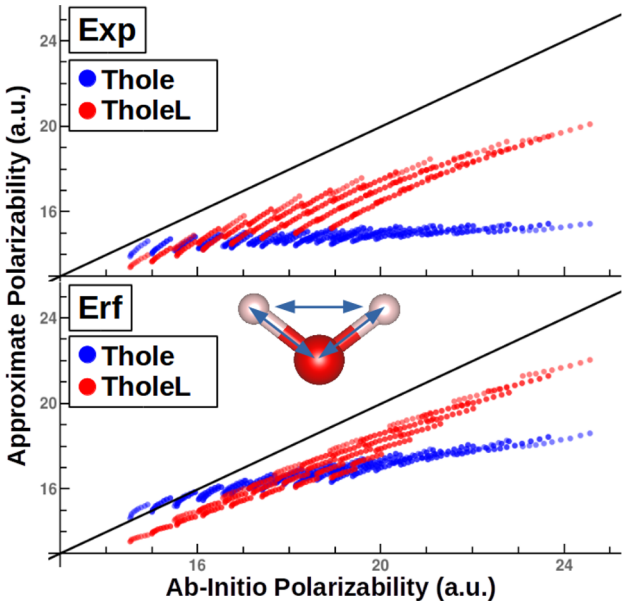

Figure 4. Polarizability of H_2O with respect to molecular configuration. The blue points are those obtained using the Thole model, while the red points are those obtained using the TholeL model.

the case with the H_2O molecule and the "Exp" dipole interaction. The TholeL model, on the other hand, improves the polarizabilities yielded by the "Exp" interaction for all molecular configurations and, with the "Erf" interaction, yields more accurate polarizabilities over essentially the entire range of sampled geometries. Thus, paired with the proper dipole interaction, the TholeL model can yield quantitatively accurate molecular polarizabilities for essentially all reasonable configurations likely to be found in molecular dynamics simulations.

To further illustrate the performance of the TholeL model, we consider a second example: a dissociating H_2 molecule. In this case, we used CCSD(T) with the dAug-cc-pVTZ basis to both optimize the H_2 geometry and calculate the polarizability. We set the r(HH) distance to the ground state value of 0.7431 Å and then sample the polarizability at distances from [−0.2 Å,2.2 Å] with respect to the ground state. We plot the longitudinal, perpendicular, and average polarizability of H_2 obtained from CCSD(T), Thole, and TholeL in Figure 5. Once again, the Thole model is qualitatively correct, reproducing the overall trends while failing to yield accurate polarizabilities far from the ground state. The TholeL model tends to overestimate changes in the longitudinal polarizability and underestimate changes in the perpendicular polarizability, but still yields excellent results for both components and the average polarizability all the way up to the dissociation point at ∼3.1 Å, especially for the "Erf" interaction. Past the point of

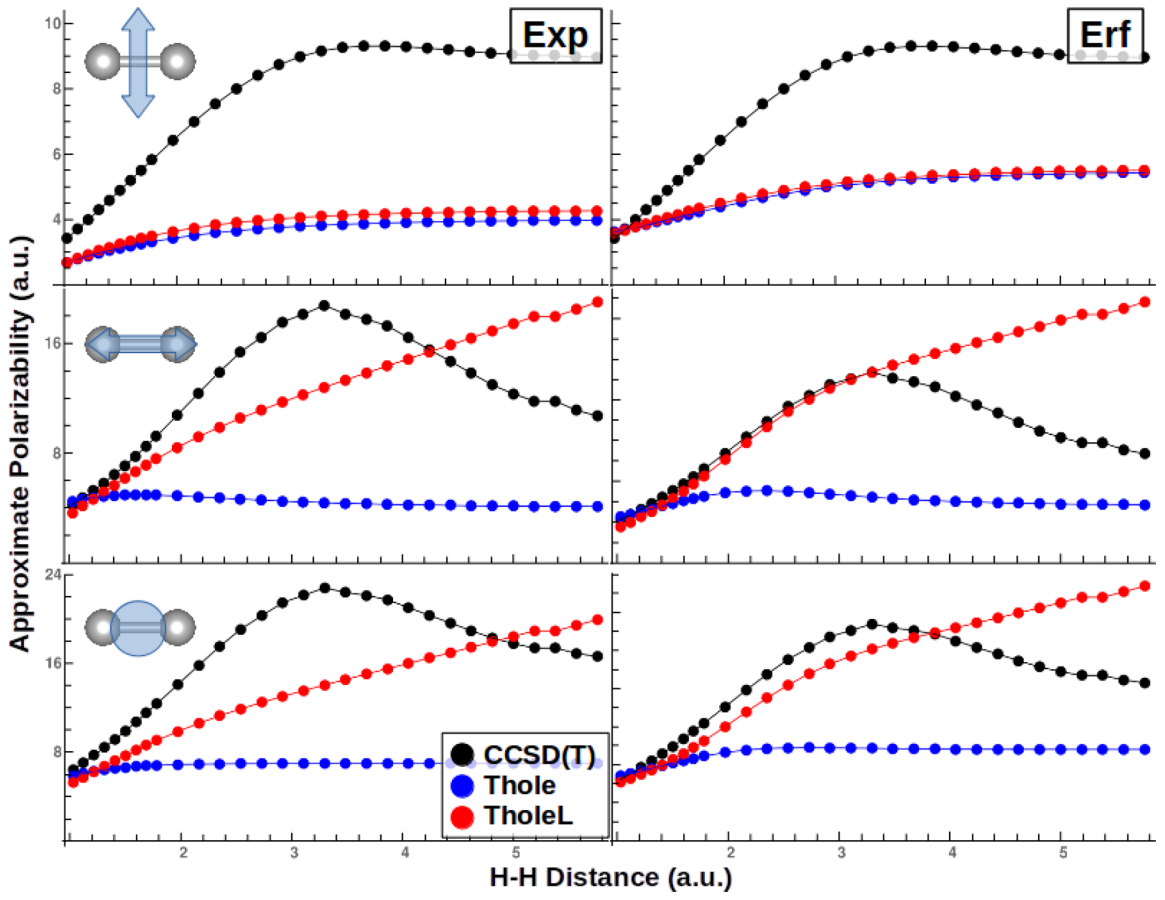

Figure 5. Polarizability of the H_2 molecule with respect to the H−H distance. The black points are calculated using CCSD(T), blue points are calculated using the Thole model, and red points are calculated using the Thole model. The panels on the left and right and computed using the "Exp" and "Erf" interaction models, respectively. The top, middle, and bottom panels show the perpendicular, longitudinal, and average polarizabilities, respectively.

DOI: 10.1021/acs.jpca.8b12011
J. Phys. Chem. A 2019, 123, 5378−5387

dissociation, the TholeL model is no longer accurate as the dependence on the interatomic distance is determined only by the nearest-neighbor distance, without any regard to bond breaking. This was to simplify the model and reduce the number of parameters by not making a reference to bond length parameters, as the intended use of the TholeL model is condensed systems. However, in Figure 5, we see that even for rather extreme bond fluctuations, the TholeL model still yields accurate results.

Since the TholeL model with the "Erf" dipole interaction yields accurate derivatives of the molecular polarizability with respect to atomic positions, the TholeL model should yield accurate Raman spectra for a wide range of systems. To test this hypothesis, we calculated Raman spectra from CPMD trajectories using the SCAN functional and the "Erf" dipole interaction for several different systems where the Raman spectrum is an important tool for characterization.

We first calculate the Raman spectrum $I_{\parallel}(\omega)$ and $I_{\perp}(\omega)$ for liquid water at 300 K from a simulation of 32 H_2O molecules in Figures 6 and 7, where we see that the TholeL model yields

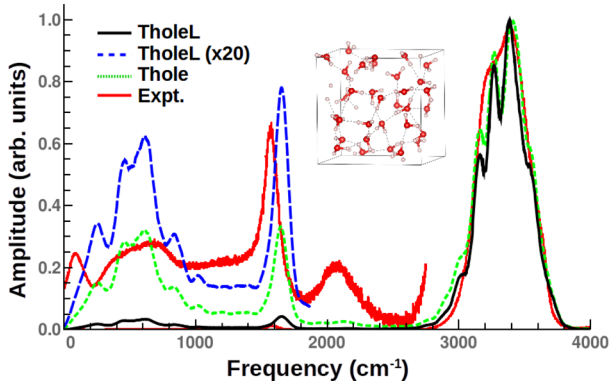

Figure 6. Raman spectrum, $I_{\parallel}(\omega)$, of water calculated from the Thole and TholeL models (normalized to unity). The black solid line is the spectrum normalized to unity, while the blue dashed line is the same multiplied by 20, and the green dashed line is the Thole spectrum. The red points show the experimental spectrum, where the region below 3000 cm^{-1} has been enlarged by a factor of roughly 100.[28]

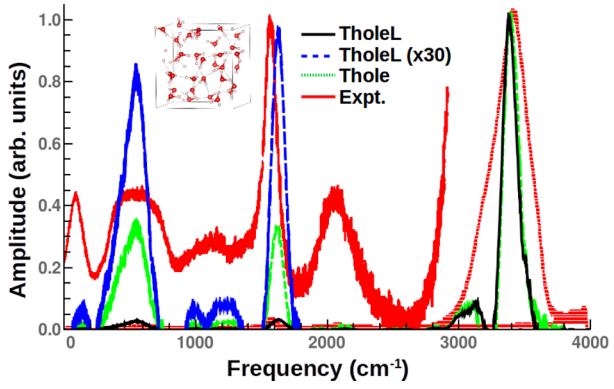

Figure 7. The Raman spectrum, $I_{\perp}(\omega)$, of water calculated from the Thole and TholeL models (normalized to unity). The black solid line is the spectrum normalized to unity, while the blue dashed line is the same multiplied by 30, and the green dashed line is the Thole spectrum. The red points show the experimental spectrum, where the region below 3000 cm^{-1} has been enlarged by a factor of roughly 100.[28]

excellent agreement with the experiment.[28] While the frequencies of the different peaks are determined from the underlying forces associated with the functional, the intensity and shape of the resulting peaks is entirely a result of the form and parameters of the TholeL model. The ratio of the intensities is remarkably close to what is observed in experiment: the O−H stretching mode (~3400 cm^{-1}) should be ~100× larger than the bending mode (~1700 cm^{-1}), though the vibrational band (~600 cm^{-1}) is slightly too large compared to the bending mode. However, we note that the agreement is excellent given the simplicity of the model we are using and is comparable to results from much more sophisticated models, for example, MB-pol.[46] Importantly, the Raman intensities are dramatically improved with respect to the Thole model, which underestimates the amplitude in the O−H stretching region by over an order of magnitude.

In order to demonstrate the generality of the TholeL model, we calculate the Raman spectrum of urea in different bonding environments. We choose to study the urea molecule as it is a well-studied test case in polarizability calculations,[18,47] and Raman spectra have been reported in a number of environments.[48−50] We plot the Raman spectrum for crystalline urea in Figure 8, with the N−H stretching region shown in Figure

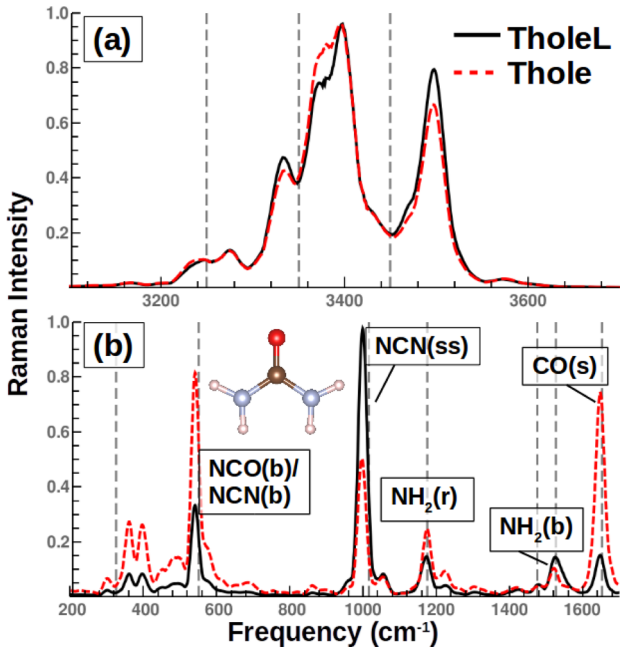

Figure 8. Calculated Raman spectrum $I_{\parallel}(\omega)$ of crystalline urea, where the solid black line and dashed red line show the TholeL and Thole spectra, respectively. The dashed vertical lines show the observed peak values.[51] All spectra have been normalized to fit on the same plot. Each panel shows a different frequency range.

8a and the C−H stretching and NH_2 bending regions shown in Figure 8b. The Thole and TholeL spectra in the N−H stretching region are quite similar, but at lower frequencies, in Figure 8b, we see significant differences between the two models. We have labeled the peaks according to the molecular motions as either bending (b), stretching (s), rocking (r), or symmetric stretching (ss). Experiments show that the NCN(ss) peak should be roughly 10 times that of the NH_2(b) and CO(s) peaks, which should be roughly equal in amplitude.[51] While the TholeL model yields intensities that roughly match

DOI: 10.1021/acs.jpca.8b12011
J. Phys. Chem. A 2019, 123, 5378−5387

the experiments, the Thole model vastly underestimates the amplitutde of the NCN(ss) peak while overestimating the amplitude of the CO(s) peak.

In addition to crystalline urea, we also computed Raman spectra for a urea molecule solvated by 32 H_2O molecules. In order to investigate the impact of solvation on the Raman spectrum, we compute the effective polarizabilities for all atoms in the system, but we plot the Raman spectra for only urea for the Thole and TholeL models in Figure 9. Once again,

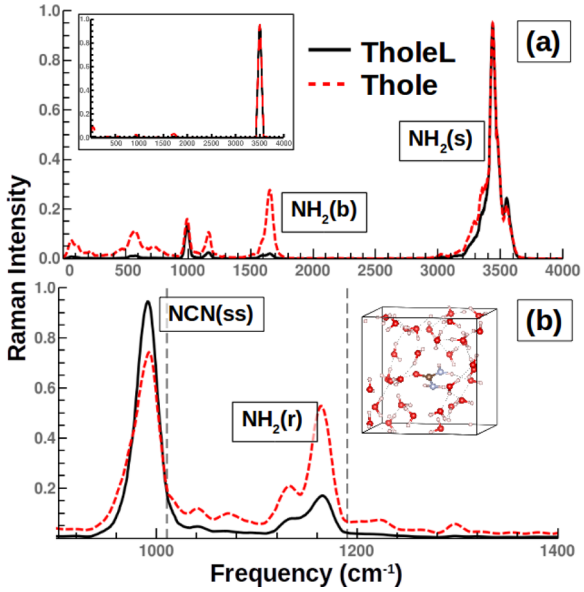

Figure 9. Calculated Raman spectrum $I_{\parallel}(\omega)$ of urea solvated by 32 H_2O molecules, where the solid black line and dashed red line show the TholeL and Thole spectra, respectively. The dashed vertical lines show the experimentally observed peak values of urea in water.[49,52] All spectra have been normalized to fit on the same plot. The inset shows the Raman spectrum of urea in vacuum.

from the bending region in Figure 9b, we see that the Thole model underestimates the amplitude of the NCN stretching peak at ~1000 cm^{-1} compared to the NH_2 bending peak at ~1175 cm^{-1}. Experiments predict that the C−N stretching peak should be roughly 10 times larger than the NH_2 rocking peak;[49,52] the TholeL model predicts a ratio of 6, while the Thole model predicts a ratio of 1.5. Figure 9a also shows that the Thole model predicts a strong CO(s) and NH_2(b) peak around 1500−1600 cm^{-1}, while both the TholeL model and experiments show that these modes only contribute a broad, low band, consistent with the experiments.[52] Thus, the TholeL model yields significant improvements for urea solvated by water in addition to crystalline urea.

CONCLUSIONS

In conclusion, we have introduced a new model for the polarizability based on the Thole model and bond-dependent atomic polarizabilities. Without adding any new parameters to the model, but simply considering the volume occupied by an atom-in-molecule and scaling the atomic polarizability by the ratio of the radius of the spherical volume to the covalent radius, we have significantly improved the generality of the Thole model. While this model violates the empirical rule that the polarizability is linearly related to the volume,[27] note that we are scaling the atom-in-molecule polarizabilities, while the empirical linear relationship has been tested primarily with molecular polarizabilities and volumes. Our approach to the "atomic volume" is a relatively simple idea that nonetheless yields excellent results for a wide range of molecules in a diverse array of configurations and condensed phase environments. By further expanding our ideas on the atomic volume in a molecule and how it impacts the polarizability and possibly other properties, even greater improvements in accuracy and generality may be possible. Even with the simple model we have introduced, however, that we are able to use the TholeL model to calculate highly accurate Raman spectra from ab initio trajectories for a diverse array of materials. With the accuracy of the TholeL model over a wide range of molecular configurations, this model might also be useful for molecular simulations, where accurate polarizabilities are required for all possible configurations of a molecule in a given ensemble.

ASSOCIATED CONTENT

Supporting Information

The Supporting Information is available free of charge on the ACS Publications website at DOI: 10.1021/acs.jpca.8b12011.

Set of molecules used to generate random configurations with CPMD, the simulation details for the CPMD simulations used to compute Raman spectra, and the optimized polarizability parameters used in all polarizability calculations (PDF)

AUTHOR INFORMATION

Corresponding Author

*E-mail: eborguet@temple.edu.

ORCID

Mark DelloStritto: 0000-0002-0678-5860

Notes

The authors declare no competing financial interest.

ACKNOWLEDGMENTS

This work was supported by the Center for Complex Materials, an Energy Frontier Research Center funded by the U.S. Department of Energy, Office of Science, Basic Energy Sciences under grant no. DE-SC0012575 and by the U.S. Army Research Laboratory under contract no. W911NF-16-2-0189. This research includes calculations carried out on Temple University's HPC resources and thus was supported in part by the National Science Foundation through major research instrumentation under grant number 1625061 and by the U.S. Army Research Laboratory under contract number W911NF-16-2-0189.

REFERENCES

(1) Brooks, B. R.; Bruccoleri, R. E.; Olafson, B. D.; States, D. J.; Swaminathan, S.; Karplus, M. CHARMM: A Program for Macromolecular Energy, Minimization, and Dynamics Calculations. *J. Comput. Chem.* **1983**, *4*, 187−217.

(2) Lamoureux, G.; MacKerell, A. D., Jr.; Roux, B. A Simple Polarizable Model of Water Based on classical Drude oscillators. *J. Chem. Phys.* **2003**, *119*, 5185−5197.

(3) Chialvo, A. A.; Cummings, P. T. Simple Transferable Intermolecular Potential for the Molecular Simulation of Water Over Wide Ranges of State Conditions. *Fluid Phase Equilib.* **1998**, *150-151*, 73−81.

(4) Warshel, A.; Kato, M.; Pisliakov, A. V. Polarizable Force Fields: History, Test Cases, and Prospects. *J. Chem. Theory Comput.* **2007**, *3*, 2034−2045.

(5) Thompson, M. A. QM/MMpol: A Consistent Model for Solute/Solvent Polarization. Application to the Aqueous Solvation and Spectroscopy of Formaldehyde, Acetaldehyde, and Acetone. *J. Phys. Chem.* **1996**, *100*, 14492−14507.
(6) McQuarrie, D. A. *Statistical Mechanics*; University Science Books: Sausalito, CA, 2000.
(7) Boyd, R. *Nonlinear Optics*; Elsevier, 2008.
(8) Shen, Y. R. *The Principles of Nonlinear Optics*; Wiley, 2003.
(9) Hickey, A. L.; Rowley, C. N. Benchmarking Quantum Chemical Methods for the Calculation of Molecular Dipole Moments and Polarizabilities. *J. Phys. Chem. A* **2014**, *118*, 3678−3687.
(10) Christiansen, O.; Halkier, A.; Koch, H.; Jørgensen, P.; Helgaker, T. Integral-Direct Coupled Cluster Calculations of Frequency-Dependent Polarizabilities, Transition Probabilities and Excited-State Properties. *J. Chem. Phys.* **1998**, *108*, 2801−2816.
(11) Wu, T.; Kalugina, Y. N.; Thakkar, A. J. Choosing a Density Functional for Static Molecular Polarizabilities. *Chem. Phys. Lett.* **2015**, *635*, 257−261.
(12) Kang, Y. K.; Jhon, M. S. Additivity of Atomic Static Polarizabilities and Dispersion Coefficients. *Theor. Chim. Acta* **1982**, *61*, 41−48.
(13) Zhou, T.; Dykstra, C. E. Additivity and Transferability of Atomic Contributions to Molecular Second Dipole Hyperpolarizabilities. *J. Phys. Chem. A* **2000**, *104*, 2204−2210.
(14) Silberstein, L. VII. Molecular Refractivity and Atomic Interaction. *The London, Edinburgh, and Dublin Philosophical Magazine and Journal of Science* **2009**, *33*, 92−128.
(15) Applequist, J.; Carl, J. R.; Fung, K.-K. Atom Dipole Interaction Model for Molecular Polarizability. Application to Polyatomic Molecules and Determination of Atom Polarizabilities. *J. Am. Chem. Soc.* **1972**, *94*, 2952−2960.
(16) Thole, B. T. Molecular Polarizabilities Calculated with a Modified Dipole Interaction. *Chem. Phys.* **1981**, *59*, 341−350.
(17) Wang, J.; Cieplak, P.; Li, J.; Hou, T.; Luo, R.; Duan, Y. Development of Polarizable Models for Molecular Mechanical Calculations I: Parameterization of Atomic Polarizability. *J. Phys. Chem. B* **2011**, *115*, 3091−3099.
(18) Jensen, L.; Sylvester-Hvid, K. O.; Mikkelsen, K. V.; Åstrand, P.-O. A Dipole Interaction Model for the Molecular Second Hyperpolarizability. *J. Phys. Chem. A* **2003**, *107*, 2270−2276.
(19) Jensen, L.; Åstrand, P.-O.; Sylvester-Hvid, K. O.; Mikkelsen, K. V. Frequency Dependent Molecular Polarizability Calculated within an Interaction Model. *J. Phys. Chem. A* **2000**, *104*, 1563−1569.
(20) Birge, R. R. Calculation of Molecular Polarizabilities Using an Anisotropic Atom Point Dipole Interaction Model which Includes the Effect of Electron Repulsion. *J. Chem. Phys.* **1980**, *72*, 5312.
(21) DelloStritto, M.; Piontek, S. M.; Klein, M. L.; Borguet, E. Relating Interfacial Order to Sum Frequency Generation with Ab Initio Simulations of the Aqueous $Al_2O_3(0001)$ and $(11\bar{2}0)$ Interfaces. *J. Phys. Chem. C* **2018**, *122*, 21284−21294.
(22) Blair, S. A.; Thakkar, A. J. TABS: A Database of Molecular Structures. *Computational and Theoretical Chemistry* **2014**, *1043*, 13−16.
(23) Jensen, L. L.; Jensen, L. Electrostatic Interaction Model for the Calculation of the Polarizability of Large Noble Metal Nanoclusters. *J. Phys. Chem. C* **2008**, *112*, 15697−15703.
(24) Mayer, A. Formulation in Terms of Normalized Propagators of a Charge-Dipole Model Enabling the Calculation of the Polarization Properties of Fullerenes and Carbon Nanotubes. *Phys. Rev. B* **2007**, *75*, No. 045407.
(25) Hirshfeld, F. L. Bonded-Atom Fragments for Describing Molecular Charge Densities. *Theor. Chim. Acta* **1977**, *44*, 129−138.
(26) Bader, R. F. W.; Henneker, W. H.; Cade, P. E. Molecular Charge Distributions and Chemical Binding. *J. Chem. Phys.* **1967**, *46*, 3341−3363.
(27) Brinck, T.; Murray, J. S.; Politzer, P. Polarizability and Volume. *J. Chem. Phys.* **1993**, *98*, 4305−4306.
(28) Brooker, M. H.; Hancock, G.; Rice, B. C.; Shapter, J. Raman Frequency and Intensity Studies of Liquid H_2O, $H_2{}^{18}O$ and D_2O. *J. Raman Spectrosc.* **1989**, *20*, 683−694.
(29) Ramìrez, R.; Lòpez-Ciudad, T.; Kumar P, P.; Marx, D Quantum Corrections to Classical Time-Correlation Functions: Hydrogen Bonding and Anharmonic Floppy Modes. *J. Chem. Phys.* **2004**, *121*, 3973−3983.
(30) Frisch, M. et al. *Gaussian16* A.03. 2016; Gaussian Inc.: Wallingford, CT.
(31) Chai, J.-D.; Head-Gordon, M. Long-Range Corrected Hybrid Density Functionals with Damped Atom-Atom Dispersion Corrections. *Phys. Chem. Chem. Phys.* **2008**, *10*, 6615−6620.
(32) Kendall, R. A.; Dunning, T. H., Jr.; Harrison, R. J. Electron Affinities of the First-Row Atoms Revisited. Systematic Basis Sets and Wave Functions. *J. Chem. Phys.* **1992**, *96*, 6796−6806.
(33) Dunning, T. H., Jr. Gaussian Basis Sets for Use in Correlated Molecular Calculations. I. The Atoms Boron Through Neon and Hydrogen. *J. Chem. Phys.* **1989**, *90*, 1007−1023.
(34) Johnson, S. G. *The NLopt Nonlinear-Optimization Package*. http://ab-initio.mit.edu/nlopt.
(35) Rowan, T. Functional Stability Analysis of Numerical Algorithms. Ph.D Thesis, University of Texas at Austin, Austin, Texas, 1990.
(36) Becke, A. D. Density-Functional Exchange-Energy Approximation with Correct Asymptotic Behavior. *Phys. Rev. A* **1988**, *38*, 3098−3100.
(37) Lee, C.; Yang, W.; Parr, R. G. Development of the Colle-Salvetti Correlation-Energy Formula into a Functional of the Electron Density. *Phys. Rev. B* **1988**, *37*, 785−789.
(38) Giannozzi, P.; et al. QUANTUM ESPRESSO: a Modular and Open-Source Software Project for Quantum Simulations of Materials. *J. Phys.: Condens. Matter* **2009**, *21*, 395502.
(39) Giannozzi, P.; et al. Advanced Capabilities for Materials Modelling with Quantum ESPRESSO. *J. Phys.: Condens. Matter* **2017**, *29*, 465901.
(40) Hamann, D. R.; Schlüter, M.; Chiang, C. Norm-Conserving Pseudopotentials. *Phys. Rev. Lett.* **1979**, *43*, 1494−1497.
(41) Vanderbilt, D. Optimally Smooth Norm-Conserving Pseudopotentials. *Phys. Rev. B* **1985**, *32*, 8412−8415.
(42) Sun, J.; Ruzsinszky, A.; Perdew, J. P. Strongly Constrained and Appropriately Normed Semilocal Density Functional. *Phys. Rev. Lett.* **2015**, *115*, No. 036402.
(43) Nosé, S. A Unified Formulation of the Constant Temperature Molecular Dynamics Methods. *J. Chem. Phys.* **1984**, *81*, 511−519.
(44) Bylander, D. M.; Kleinman, L. Energy Fluctuations Induced by the Nosé Thermostat. *Phys. Rev. B* **1992**, *46*, 13756−13761.
(45) Applequist, J. Atom Charge Transfer in Molecular Polarizabilities: Application of the Olson-Sundberg Model to Aliphatic and Aromatic Hydrocarbons. *J. Phys. Chem.* **1993**, *97*, 6016−6023.
(46) Medders, G. R.; Paesani, F. Infrared and Raman Spectroscopy of Liquid Water through "First-Principles" Many-Body Molecular Dynamics. *J. Chem. Theory Comput.* **2015**, *11*, 1145−1154.
(47) Pluta, T.; Sadlej, A. J. Electric Properties of Urea and Thiourea. *J. Chem. Phys.* **2001**, *114*, 136−146.
(48) Keuleers, R.; Desseyn, H. O.; Rousseau, B.; Van Alsenoy, C. Vibrational Analysis of Urea. *J. Phys. Chem. A* **1999**, *103*, 4621−4630.
(49) Hoccart, X.; Turrell, G. Raman Spectroscopic Investigation of the Dynamics of Urea Water Complexes. *J. Chem. Phys.* **1993**, *99*, 8498−8503.
(50) Langer, J.; Schrader, B.; Bastian, V.; Jacob, E. Infrared Spectra and Force Constants of Urea in the Gaseous Phase. *Fresenius' J. Anal. Chem.* **1995**, *352*, 489−495.
(51) Frost, R. L.; Kristof, J.; Rintoul, L.; Kloprogge, J. T. Raman Spectroscopy of Urea and Urea-Intercalated Kaolinites at 77 K. *Spectrochim. Acta, Part A* **2000**, *56*, 1681−1691.
(52) Wen, N.; Brooker, M. H. Urea protonation: Raman and Theoretical Study. *J. Phys. Chem.* **1993**, *97*, 8608−8616.

DOI: 10.1021/acs.jpca.8b12011
J. Phys. Chem. A 2019, 123, 5378−5387